Sol-gel loading of $Sm_2Ti_2O_7$ on HZSM-5 zeolite for enhanced photocatalytic activity

JUN YAO, YANGYANG CHEN, LING DU, WENJIE ZHANG*
School of science, Shenyang Ligong University, Shenyang 110159, China

$Sm_2Ti_2O_7$/HZSM-5 composite material was prepared by sol-gel method. Pyrochlore structured $Sm_2Ti_2O_7$ formed in the unloaded $Sm_2Ti_2O_7$ and $Sm_2Ti_2O_7$/HZSM-5. EDS mappings of Sm and Ti prove the loading of $Sm_2Ti_2O_7$ on the surface of HZSM-5. Typical absorptions of $Sm_2Ti_2O_7$ appear in the infrared spectra of the $Sm_2Ti_2O_7$/HZSM-5 samples calcined at temperature over 800 °C. The maximum amount of hydroxyl radicals is produced on the $Sm_2Ti_2O_7$/HZSM-5 sample calcined at 800 °C. E_{CB} and E_{VB} of $Sm_2Ti_2O_7$/HZSM-5 at 800 °C are -0.66 V and 2.77 V, respectively. The supported $Sm_2Ti_2O_7$/HZSM-5 has much improved activity as compared to the unloaded $Sm_2Ti_2O_7$.

(Received December 4, 2017; accepted February 12, 2019)

Keywords: $Sm_2Ti_2O_7$, HZSM-5, Sol-gel, Photocatalytic, Degradation

1. Introduction

The promising progress in photocatalytic technology has made it a potential advanced oxidation method in dealing with environmental organic pollutants [1,2]. Photocatalytic material is the key factor in applying this technique [3,4]. Although TiO_2 matrix materials are the most widely used photocatalysts [5,6], researchers have paid much attention to other types of materials such as titanates. Titanates are classified by the cation element in the chemical formula, i.e. alkaline earth metal, transition metal and rare earth elements [7-9]. Pyrochloro structured $Sm_2Ti_2O_7$ has been reported as photocatalyst on removal of organic pollutants, as well as the activity on water splitting to generate hydrogen [10-12].

Since titanates are usually prepared at high temperature, the materials are lack of porous structure and surface area. This property limits adsorption capacity and photocatalytic activity of titanates. PEG4000 was used as template in sol-gel synthesizing of porous $Sm_2Ti_2O_7$ in our previous work [13]. HZSM-5 zeolite was used to support $Gd_2Ti_2O_7$ [14] and $La_2Ti_2O_7$ [15]. Photocatalytic activities of the titanates are greatly promoted after loading on the surface of HZSM-5 zeolite.

HZSM-5 zeolite is well known for its large surface area and microporous structure. In this work, $Sm_2Ti_2O_7$/HZSM-5 material was prepared by sol-gel method. $Sm_2Ti_2O_7$ was loaded on the surface of HZSM-5 zeolite. The $Sm_2Ti_2O_7$/HZSM-5 samples were characterized by X-ray diffraction, scanning electron microscope and infrared absorption spectra. Photocatalytic degradation of Reactive Brilliant Red X-3B (RBR X-3B) and hydroxyl radical generation were examined to determine photocatalytic activity of $Sm_2Ti_2O_7$/HZSM-5.

2. Experimental

2.1. Preparation of $Sm_2Ti_2O_7$/HZSM-5

$Sm_2Ti_2O_7$ was loaded on HZSM-5 through a sol-gel route. Two solutions were prepared in advance. Samarium nitrate, acetic acid and deionized water were mixed to prepare the first solution. Tetrabutyl titanate was dissolved in ethanol to prepare the second solution. The solutions were mixed together to form a transparent sol, followed by addition of HZSM-5 powders. The n(Sm)/n(Ti) molar ratio in the precursor was 1:1. Gel formed after 60 min stirring in a 50 °C water bath. The gel was dried at 110 °C for 15 h, and then calcined at 800 °C for 3 h. Weight percent of $Sm_2Ti_2O_7$ in the $Sm_2Ti_2O_7$/HZSM-5 composite was 70%.

2.2. Characterization methods

X-ray diffraction pattern was determined by a D8 Advance X-ray diffractometer. Monochromatized Cu Kα was chosen as the initial radiation source at λ=0.15416 nm. Surface morphology of the material was observed on QUANTA 250 scanning electron microscope. The surface of the sample is pre-coated with a thin layer of gold before measuring. Infrared absorption spectra were recorded by a Frontier FT-IR/FIR spectrometer between 50 cm^{-1} and 4000 cm^{-1}.

2.3. Photocatalytic activity measurements

Two ways are used to measure photocatalytic activity of the $Sm_2Ti_2O_7$/HZSM-5 composite. Hydroxyl radical produced during photocatalytic process was measured by a Hitachi F-2500 fluorescence spectrophotometer. A 20 W UV-light lamp irradiates at 253.7 nm with 1300 μW/cm^2.

50 mL 0.5 mmol/L terephthalic acid solution and 20 mg $Sm_2Ti_2O_7$ were mixed in a 100 mL quartz beaker. The mixture was illuminated for 30 min. The solid photocatalyst and the solution were subsequently filtrated. The solution was excited in the fluorescence spectrophotometer at 315 nm. The fluorescence intensity of 2-hydroxyterephthalic acid was measured from 360 nm to 540 nm.

Photocatalytic degradation of RBR X-3B was examined. 20 mg $Sm_2Ti_2O_7$ and 50 mL 30 mg/L RBR X-3B solution were stirred in the dark for 30 min. Adsorption percentage of RBR X-3B on $Sm_2Ti_2O_7$/HZSM-5 was analyzed after adsorption-desorption equilibrium. Photocatalytic oxidation was conducted for 30 min as well. Concentration of RBR X-3B solution was measured on a 721E spectrophotometer at 537.6 nm.

3. Results and discussion

Fig. 1 shows X-ray diffraction patterns of HZSM-5, $Sm_2Ti_2O_7$ and $Sm_2Ti_2O_7$/HZSM-5. Pyrochlore structured $Sm_2Ti_2O_7$ exists in the unloaded $Sm_2Ti_2O_7$ sample and $Sm_2Ti_2O_7$/HZSM-5. There is no other phase of samarium titanate in the materials. The diffraction pattern of $Sm_2Ti_2O_7$ is the same to that of JCPDS No.73-1699. The strongest diffraction peak at 30^o indicates the most preferred (222) plane. The diffraction pattern of HZSM-5 presents a complex combination of tetrahedral Si-O and Al-O skeletons. Both of the diffraction peaks of $Sm_2Ti_2O_7$ and HZSM-5 zeolite are found in the pattern of $Sm_2Ti_2O_7$/HZSM-5. Since weight percent of $Sm_2Ti_2O_7$ in the $Sm_2Ti_2O_7$/HZSM-5 composite is 70%, very weak diffraction peaks of HZSM-5 can be distinguished in the pattern of $Sm_2Ti_2O_7$/HZSM-5. The $Sm_2Ti_2O_7$ and $Sm_2Ti_2O_7$/HZSM-5 in the figure is produced at 800 ^oC. The $Sm_2Ti_2O_7$ layer is coated on the surface of HZSM-5 particles. Apparently, the HZSM-5 zeolite does not put much effect on crystallization of $Sm_2Ti_2O_7$.

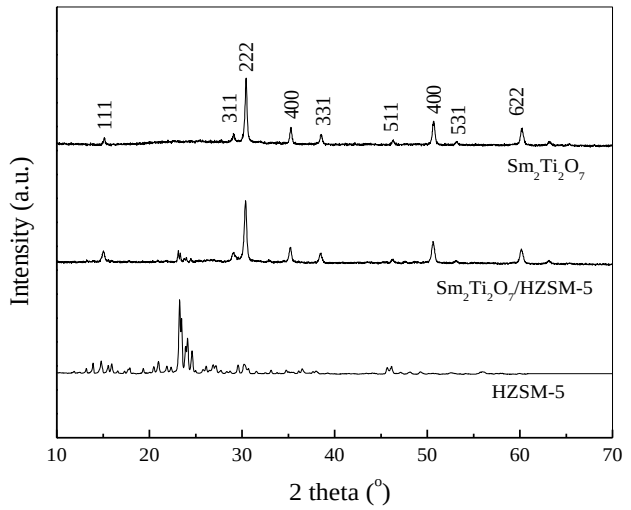

Fig. 1. XRD patterns of $Sm_2Ti_2O_7$ and $Sm_2Ti_2O_7$/HZSM-5. The materials were prepared at 800 ^oC

Fig. 2 shows surface morphology of $Sm_2Ti_2O_7$/HZSM-5 and EDS mappings of Sm and Ti on the sample. The HZSM-5 particles are coated by a layer of $Sm_2Ti_2O_7$, so that the original shape of HZSM-5 particles cannot be identified. Surface morphology of the $Sm_2Ti_2O_7$/HZSM-5 composite is rough. EDS mappings of Sm and Ti on the material prove the distribution of Sm and Ti elements on the surface of $Sm_2Ti_2O_7$/HZSM-5. As can be seen from the figure, $Sm_2Ti_2O_7$ is well distributed on the HZSM-5 particles.

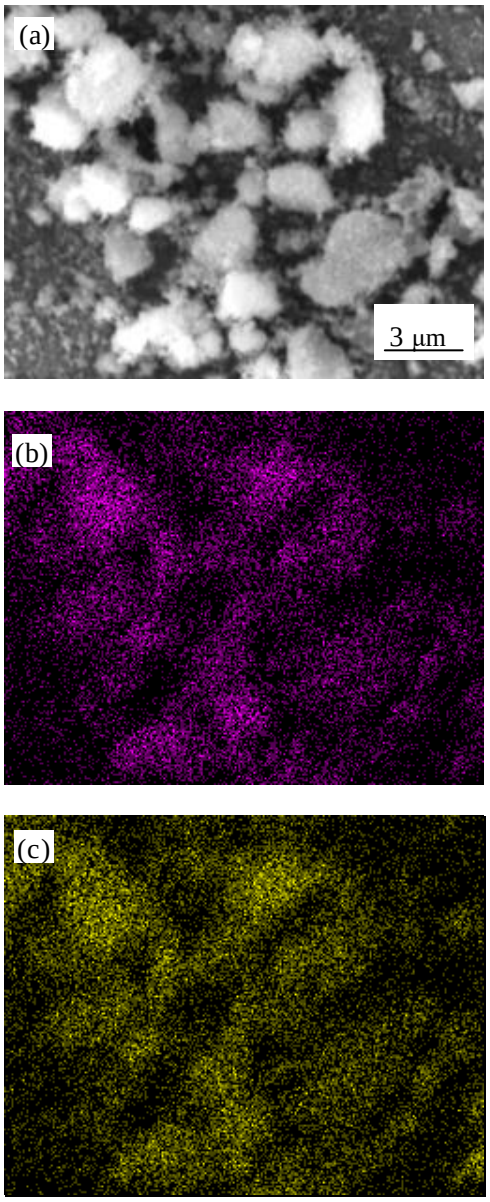

Fig. 2. Surface morphology of $Sm_2Ti_2O_7$/HZSM-5 and EDS mappings of Sm and Ti. (a) SEM image, (b) Sm, (c) Ti

Fig. 3 presents infrared and far infrared spectra of $Sm_2Ti_2O_7$/HZSM-5 at different calcination temperatures. The typical absorptions of the material can be used to show the bonding characters in the sample. Stretching

vibrations of Si-OH and Al-OH in HZSM-5 have absorptions at 3882 cm^{-1} and 3706 cm^{-1} when calcination temperature is below 700 °C [16]. The absorptions disappear at high temperature after polycondensation of the surface hydroxyl groups. The surface adsorbed water molecules are reduced at high temperature, leading to shrinking absorption peaks of hydroxyl stretching vibration at 3440 cm^{-1} and 1634 cm^{-1}. The antisymmetric stretching vibration of Al-O-Al or Si-O-Si situates at 1232 cm^{-1}, while the vibration of tetrahedral SiO_4 ring are at 1099 cm^{-1} and 783 cm^{-1} [17].

As shown in Fig. 3(b), far infrared absorptions of metal oxide bondings in the materials prove the existence of $Sm_2Ti_2O_7$. The absorption peaks at 448 cm^{-1} and 383 cm^{-1} are attributed to stretching vibration of Sm-O [18]. Stretching vibration of Sm-TiO_6 situates at 248 cm^{-1}. The absorption at 297 cm^{-1} is due to bending vibration of O-Ti-O [19]. The typical absorptions of $Sm_2Ti_2O_7$ do not appear in the spectra of the samples calcined at low temperatures. The formation of $Sm_2Ti_2O_7$ occurs at temperature higher than 800 °C. The strong absorption peaks at 551 cm^{-1} and 450 cm^{-1} are related to antisymmetric stretching vibration of double pentacyclic ring in HZSM-5 and bending vibration of tetrahedral Si-O bond [20]. These two absorption peaks are weakened and broadened after raising calcination temperature, due to the effect of $Sm_2Ti_2O_7$ crystallization at high temperature.

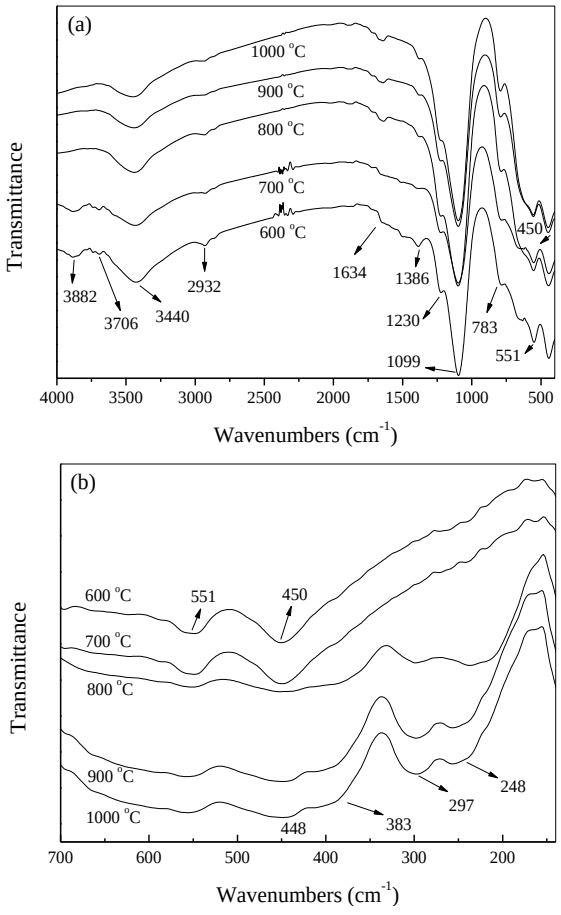

Fig. 3. FT-IR (a) and FT-FIR (b) spectra of $Sm_2Ti_2O_7$/HZSM-5 at different calcination temperatures

Photocatalytic activity of photocatalyst can be evaluated by the amount of hydroxyl radicals produced during illumination. Hydroxyl radical can react with terephthalic acid to produce 2-hydroxyterephthalic acid [21]. The concentration of 2-hydroxyterephthalic acid can be analyzed based on its fluorescence property. Photocatalytic activity of $Sm_2Ti_2O_7$/HZSM-5 samples calcined at different temperatures is measured in this way. Photoluminescence spectra of the 2-hydroxyterephthalic acid solution after excitation are shown in Fig. 4. The fluorescence emitting spectra of 2-hydroxyterephthalic acid centering at 425 nm is proportional to its concentration in the solution. As can be seen from the figure, the maximum amount of hydroxyl radicals can be produced on the $Sm_2Ti_2O_7$/HZSM-5 sample calcined at 800 °C.

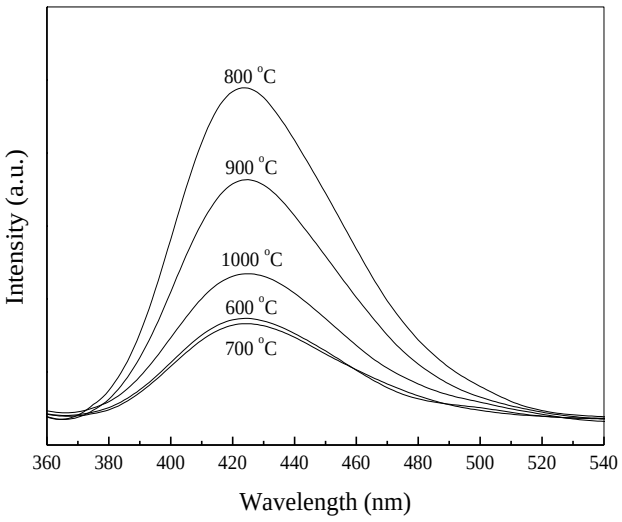

Fig. 4. Hydroxyl radical formation on $Sm_2Ti_2O_7$/HZSM-5 at different calcination temperatures. The irradiation time was 30 min

The edges of conduction band and valence band can be calculated through equations [22,23],

$$E_{CB} = X - E^C - 1/2Eg, \text{ and } E_{VB} = E_{CB} + Eg,$$

where E_{CB} and E_{VB} are the positions of conduction band edge and valence band edge, X is the absolute electronegativity of the semiconductor, Eg is the band gap of the semiconductor and E^C is the energy of free electrons on the hydrogen scale. The band gap energy of $Sm_2Ti_2O_7$/HZSM-5 calcined at 800 °C is 3.43 eV [24], so that E_{CB} and E_{VB} are -0.66 V and 2.77 V, respectively. Fig. 5 presents the schematic illustration of photocatalytic exciting mechanism on $Sm_2Ti_2O_7$/HZSM-5. Since the oxidation potentials are 2.72 V and 1.89 V（NHE）to oxidize H_2O and OH^- to •OH radicals, photogenerated holes can directly oxidize H_2O into hydroxyl radical [25]. The E_{VB} of $Sm_2Ti_2O_7$/HZSM-5 is negative to reduction potential of O_2 (-0.13 V). O_2 can be reduced to O_2^-• by photogenerated electrons [26]. The HZSM-5 can control

electron transfer from $Sm_2Ti_2O_7$ to the zeolite so as to extend the lifetime of electrons and holes [27].

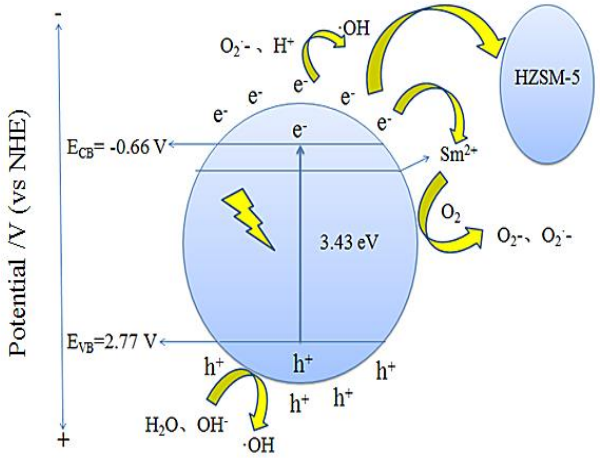

Fig. 5. Schematic illustration of photocatalytic exciting mechanism on $Sm_2Ti_2O_7$/HZSM-5

Photocatalytic activity and reusability of $Sm_2Ti_2O_7$ and $Sm_2Ti_2O_7$/HZSM-5 on RBR X-3B degradation are shown in Fig. 6. The materials are reused after each cycle of photocatalytic degradation of RBR X-3B. Photocatalytic oxidation time was 30 min in each cycle. The supported $Sm_2Ti_2O_7$/HZSM-5 has much improved activity as compared to the unloaded $Sm_2Ti_2O_7$. The degradation efficiency on $Sm_2Ti_2O_7$/HZSM-5 reduces from 34.1% to 25.0% on $Sm_2Ti_2O_7$/HZSM-5, while the efficiency is still much better than the unloaded $Sm_2Ti_2O_7$. The reducing activity of the reused $Sm_2Ti_2O_7$/HZSM-5 is mainly due to loss of fine particles during recycle of the material. Meanwhile, there might be residues on the photocatalyst after degrading RBR X-3B. The residues may be adsorbed on the surface of the material and prohibit absorption of irradiating photons.

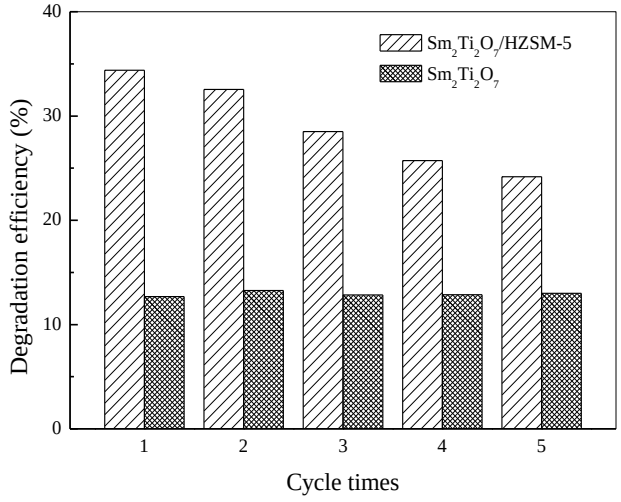

Fig. 6. Reusability of $Sm_2Ti_2O_7$ and $Sm_2Ti_2O_7$/HZSM-5 for photocatalytic degradation of RBR X-3B. The irradiation time was 30 min in each cycle

4. Conclusions

Pyrochlore structured $Sm_2Ti_2O_7$ was loaded on the surface of HZSM-5 zeolite to prepare composite $Sm_2Ti_2O_7$/HZSM-5. HZSM-5 zeolite does not put much effect on crystallization of $Sm_2Ti_2O_7$. Chemical bondings in both $Sm_2Ti_2O_7$ and HZSM-5 have absorptions in the infrared and far infrared spectra of $Sm_2Ti_2O_7$/HZSM-5. The $Sm_2Ti_2O_7$/HZSM-5 sample calcined at 800 °C can produce the maximum amount of hydroxyl radicals. E_{CB} and E_{VB} of $Sm_2Ti_2O_7$/HZSM-5 calcined at 800 °C are -0.66 V and 2.77 V, respectively. Photocatalytic degradation efficiency on $Sm_2Ti_2O_7$/HZSM-5 is greatly promoted after loading $Sm_2Ti_2O_7$ on HZSM-5.

Acknowledgments

This work was supported by the Natural Science Foundation of Liaoning Province (No. 2015020186).

References

[1] M. R. Hoffmann, S. T. Martin, W. Choi, W. Bahnemann, Chem. Rev. **95**, 69 (1995).
[2] R. Saravanan, H. Shankar, T. Prakash, V. Narayanan, Mater. Chem. Phys. **125**, 277 (2011).
[3] W. Zhang, Y. Tao, C. G Li, Mater. Res. Bull. **105**, 55 (2018).
[4] W. Zhang, J. Yang, C. Li, Mater. Sci. Semicond. Process. **85**, 33 (2018).
[5] W. J. Zhang, K. L. Wang, Y. Yu, H. B. He, Chem. Eng. J. **163**, 62 (2010).
[6] W. J. Zhang, Y. X. Liu, X. B. Pei, X. J. Chen, J. Phys. Chem. Solids **104**, 45 (2017).
[7] J. Chen, S. Liu, L. Zhang, N. Chen, Mater. Lett. **150**, 44 (2015).
[8] Y. X. Li, G Chen, H. J. Zhang, Z. H. Li, J. X. Sun, J. Solid State Chem. **181**, 2653 (2008).
[9] W. J. Zhang, Y. X. Liu, C. G Li, J. Phys. Chem. Solids **118**, 144 (2018).
[10] M. Uno, A. Kosuga, M. Okui, K. Horisaka, S. Yamanaka, J. Alloys Compd. **400**, 270 (2005).
[11] A. Ishikawa, T. Takata, T. Matsumura, J. N. Kondo, M. Hara, H. Kobayashi, K. Domen, J. Phys. Chem. B **108**, 2637 (2004).
[12] A. Nashim, K. M. Parida, Chem. Eng. J. **215-216**, 608 (2013).
[13] W. J. Zhang, Y. J. Tao, C. G Li, Solid State Sci. **78**, 16 (2018).
[14] W. J. Zhang, Y. J. Tao, C. G Li, J. Photochem. Photobio. A: Chem. **364**, 787 (2018).
[15] W. J. Zhang, Z. Ma, L. Du, L. L. Yang, X. J. Chen, H. B. He, J. Alloys Compds. **695**, 3541 (2017).
[16] K. Góra-Marek, K. Brylewska, K. A. Tarach, Appl. Catal. B **179**, 589 (2015).
[17] W. Zhang, F. Bi, Y. Yu, H. He, J. Mole. Catal. A **372**, 6 (2013).
[18] P. P. Rao, S. J. Liji, K. R. Nair, Mater. Lett. **58**, 1924

(2004).
[19] J. A. Alonso, E. Mzayek, I. Rasines, M. Ventanilla, Inorg. Chim. Acta **140**, 145 (1987).
[20] X. Li, B. S. Li, J. Q. Xu, Q. Wang, X. Pang, X. Gao, Z. Zhou, J. Piao, Appl. Clay Sci. **50**, 81 (2010).
[21] W. Zhang, H. L. Li, Z. Ma, H. Li, H. Wang, Solid State Sci. **87**, 58 (2019).
[22] H. Arthur, J. Nethercot, Phys. Rev. Lett. **33**, 1088 (1974).
[23] G Zhang, W. Zhang, J. C. Crittenden, Chin. J. Catal. **34**, 1926 (2013).
[24] W. Zhang, J. Yang, L. Du, Curr. Nanosci. **14**, 17 (2018).
[25] T. Tachikawa, M. Fujitsuka, T. Majima, J. Phys. Chem. C **111**, 5259 (2007).
[26] T. Arai, M. Yanagida, Y. Konishi, J. Phys. Chem. C **111**, 7574 (2007).
[27] M. A. O'Neill, F. L. Cozens, N. P. J. Schepp, Phys. Chem. B **105**, 12746 (2001).

*Corresponding author: wjzhang@aliyun.com